DISSERTATION

EMERGENT TOPOLOGICAL PHENOMENA IN LOW-D SYSTEMS INDUCED BY GAUGE POTENTIALS

Submitted by

Aidan Winblad

Department of Physics

In partial fulfillment of the requirements

For the Degree of Doctor of Philosophy

Colorado State University

Fort Collins, Colorado

Fall 2023

Doctoral Committee:

Advisor: Hua Chen

Richard Eykholt
Martin Gelfand
Olivier Pinaud

ABSTRACT

EMERGENT TOPOLOGICAL PHENOMENA IN LOW-D SYSTEMS INDUCED BY GAUGE POTENTIALS

Abstract goes here

ACKNOWLEDGEMENTS

I would like to thank the CSU Graduate Student Council and the CSU Graduate School for initiating, commissioning and supporting this project. I would also like to thank Nicole Ramo for her support and ensuring that we followed through with this project to completion. I would like to thank Leif Anderson, who created and supported the previous LaTeX template for a number of years. Although I have never met Leif, his work was invaluable in the creation of this package and has helped many students get their thesis approved by the CSU graduate school. Finally, I would like to thank everyone who helps to contribute to this package. Your work will help many CSU graduate students to create professional, beautiful and compelling theses and dissertations using LaTex. Last but not least, thank you to the creators and maintaners of LaTeX for creating a fantastic typesetting tool.

DEDICATION

I would like to dedicate this dissertation to my dog Zeta.

TABLE OF CONTENTS

LIST OF TABLES

LIST OF FIGURES

Chapter 1

Introduction

EM gauge potential appears in electronic Hamiltonian in CM

1. Review Maxwell theory -> gauge potential
2. Minimal coupling $-i\hbar\nabla \to -i\hbar\nabla + q\mathbf{A}$ or $-i\partial_\mu \to -i\partial_\mu + qA_\mu$
3. TB Hamiltonian and Peierls phase

Topological phenomena in CM considered in thesis

1. (1) Majorana and TSC
   - i Kitaev chain (M— topological invariant). BdG?
   - ii Braiding (Application in TQC)
2. Landau Level and Hofstadter butterfly
   - i solve for LL in 2DEG — why it's topological, chern number, TKNN quantum Hall
   - ii square lattice — hofstadter butterfly (on other lattices, honeycomb)

STUFF

Chapter 2

Superconducting Triangular Islands as a Platform for Manipulating Majorana Zero Modes

1. Introduction
2. Formalism
   i BdG — decide how much detail on derivation
   ii Majorana Number
   iii Many-Body Berry Phase
3. Model, results (uniform and non-uniform)
4. Discussion, future

2.1 Kitaev Triangle and Peierls substitution

We start with a spinless or spin-polarized p-wave superconductor

$$\mathcal{H} = \sum_{\langle j,l \rangle} (-t c_j^\dagger c_l + \Delta e^{i\theta_{jl}} c_j c_l + h.c.) - \sum_j \mu c_j^\dagger c_j, \tag{2.1}$$

where t is the hopping amplitude, Δ is the amplitude of (2D) p-wave pairing, μ is the chemical potential, θ_{jl} is the polar angle of $\mathbf{r}_{jl} = \mathbf{r}_l - \mathbf{r}_j$, consistent with $\{c_l^\dagger, c_j^\dagger\} = 0$.

We will now include a gauge potential via a Peierls substitution as

$$c_j^\dagger \to c_j^\dagger \exp\left(-\frac{ie}{\hbar}\int_0^{\mathbf{r}_j} \mathbf{A}\cdot d\mathbf{l}\right),$$

$$c_j^\dagger c_l \to c_j^\dagger c_l \exp\left(\frac{ie}{\hbar}\int_{\mathbf{r}_j}^{\mathbf{r}_l} \mathbf{A}\cdot d\mathbf{l}\right)$$

$$\to c_l^\dagger c_j e^{i\phi_{j,l}}.$$

$$\phi_{jl} = \frac{e}{\hbar}\int_{\mathbf{r}_j}^{\mathbf{r}_l} \mathbf{A}\cdot d\mathbf{l} = -\phi_{lj} \tag{2.2}$$

The modified Hamiltonian is then

$$\mathcal{H} = \sum_{\langle j,l\rangle}(-te^{i\phi_{jl}}c_j^\dagger c_l + \Delta e^{i\theta_{jl}}c_j c_l + h.c.) - \sum_j \mu c_j^\dagger c_j, \tag{2.3}$$

The complex fermion operator can be written in the Majorana Fermion basis, a superposition of two Majorana fermions $c_j = \frac{1}{2}(a_j + ib_j)$. Due to the nature of Majorana fermions, $a_j^\dagger = a_j$, the creation operator is $c_j^\dagger = \frac{1}{2}(a_j - ib_j)$. It is quickly seen after substitution we arrive at

$$c_j^\dagger c_j = \frac{1}{2}(1 + ia_j b_j), \tag{2.4}$$

$$c_j^\dagger c_l = \frac{1}{4}(a_j a_l + b_j b_l + ia_j b_l - ib_j a_l), \tag{2.5}$$

$$c_j c_l = \frac{1}{4}(a_j a_l - b_j b_l + ia_j b_l + ib_j a_l). \tag{2.6}$$

The hopping term in MF basis are

$$-t(e^{i\phi_{jl}}c_j^\dagger c_l + e^{-i\phi_{jl}}c_l^\dagger c_j) = -\frac{it}{2}(\sin\phi_{jl}(a_j a_l + b_j b_l) + \cos\phi_{jl}(a_j b_l - b_j a_l)), \tag{2.7}$$

the order parameter terms are

$$\Delta(e^{i\theta_{jl}}c_j^\dagger c_l^\dagger + e^{-i\theta_{jl}}c_j c_l) = \frac{i\Delta}{2}(\sin\theta_{jl}(a_l a_j - b_l b_j) + \cos\theta_{jl}(a_l b_j + b_l a_j)). \tag{2.8}$$

Our Hamiltonian in MF basis is then

$$\begin{aligned}\mathcal{H} = -\frac{i}{2}\sum_{\langle j,l\rangle}[&(t\sin\phi_{jl} - \Delta\sin\theta_{jl})a_j a_l + (t\sin\phi_{jl} + \Delta\sin\theta_{jl})b_j b_l \\ &+(t\cos\phi_{jl} - \Delta\cos\theta_{jl})a_j b_l - (t\cos\phi_{jl} + \Delta\cos\theta_{jl})b_j a_l] \\ -\frac{i\mu}{2}\sum_j a_j b_j\end{aligned} \tag{2.9}$$

For concreteness we consider a 1-D chain in the Kitaev limit $t = \Delta$, $\mu = 0$, and choose $phi_{jl} = 0$ (either zero or a perpendicular gauge potential). The Kitaev chain is resultant with $\mathcal{H} = \sum_{j,j+1} -itb_j a_{j+1}$ and hosting MZM a_1 and b_N.

2.2 Conditions for MZMs on equilateral triangular islands

We want to now use a gauge potential to tune our system into having zero modes located at the base corners of a triangular lattice. Consider first forming a minimal Kitaev triangle in the positive *y*-axis, with only 3-sites such that its base, with sites 1 and 2, are along the *x*-axis. While still considering the Kitaev limit in this minimal model, as previously stated, sites 1 and 2 form a Kitaev chain. In order for the MZM to persist in the presence of site 3, one can choose ϕ_{23} and ϕ_{31} so that all terms involving these Majorana operators cancel out. For example, consider the 2–3 bond, for which $\theta_{23} = 2\pi/3$, we require

$$\sin\phi_{jl} + \sin\frac{2\pi}{3} = \cos\phi_{jl} + \cos\frac{2\pi}{3} = 0 \tag{2.10}$$

which means $\phi_{23} = -\pi/3$. Similarly one can find $\phi_{31} = -\phi_{13} = -\pi/3$. The three Peierls phases can be realized by the following staggered vector potential

$$\mathbf{A} = [1 - 2\Theta(x)]\frac{2\pi}{3\sqrt{3}}\hat{\mathbf{y}}. \tag{2.11}$$

Which is derived in the following subsection

2.2.1 Staggered vector potential

First, naively consider a constant vector potential field. For sites 1–2 we want the field to be perpendicular to their axis this tells usto start with $\mathbf{A} = A\hat{\mathbf{y}}$. From Eq. 2.2, set $e = \hbar = 1$ and the path integral for ϕ_{13} becomes

$$\begin{aligned}
\phi_{13} &= \int_{\mathbf{r_1}}^{\mathbf{r_3}} \mathbf{A} \cdot d\mathbf{l} \\
&= A\int_{y_1}^{y_3} \hat{\mathbf{y}} \cdot d\mathbf{l} \\
&= A\int_{0}^{\sqrt{3}a/2} dy \\
&= \frac{\sqrt{3}Aa}{2} \\
&= \pi/3.
\end{aligned}$$

We find that we need

$$A = \frac{2\pi}{3\sqrt{3}a}. \tag{2.12}$$

Now let us check if this allows for $\phi_{23} = -\pi/3$.

$$\begin{aligned}
\phi_{23} &= \int_{\mathbf{r_2}}^{\mathbf{r_3}} \mathbf{A} \cdot d\mathbf{l} \\
&= A \int_{y_2}^{y_3} \hat{\mathbf{y}} \cdot d\mathbf{l} \\
&= A \int_{0}^{\sqrt{3}a/2} dy \\
&= \frac{\sqrt{3}Aa}{2} \\
&= \frac{\sqrt{3}a}{2} \frac{2\pi}{3\sqrt{3}a} \\
&= \pi/3 \neq -\pi/3.
\end{aligned}$$

Here we see that a constant vector potential does not meet the condition for MZMs, it's off by a sign factor. This is remedied by using the Heaviside function instead from equation 2.11

$$\mathbf{A} = [1 - 2\Theta(x)] \frac{2\pi}{3\sqrt{3}} \hat{\mathbf{y}}.$$

2.2.2 Linear vector potential

While the simplest vector potential one can use in the minimal Kitaev triangle is a staggered potential it remains to be seen if other odd functions also work. Again, we want the Peierls phase

for sites 1–2 to have no contribution, let $\mathbf{A} = Ax\hat{\mathbf{y}}$. Simlarly, for sites 1–3 we have

$$\begin{aligned}
\phi_{13} &= \int_{\mathbf{r_1}}^{\mathbf{r_3}} \mathbf{A} \cdot d\mathbf{l} \\
&= \int_{y_1}^{y_3} Axdy \\
&= \int_{x_1}^{x_3} Ax\frac{dy}{dx}dx \\
&= \sqrt{3}A\int_{-a/2}^{0} xdx \\
&= -\frac{\sqrt{3}Aa^2}{8} \\
&= \pi/3.
\end{aligned}$$

The magnitude is then

$$A = -\frac{8\pi}{3\sqrt{3}a^2}. \tag{2.13}$$

Check if $\phi_{23} = -\pi/3$:

$$\begin{aligned}
\phi_{23} &= \int_{x_2}^{x_3} Ax\frac{dy}{dx}dx \\
&= -\sqrt{3}A\int_{a/2}^{0} xdx \\
&= A\left(\frac{\sqrt{3}a^2}{8}\right) \\
&= -\frac{8\pi}{3\sqrt{3}a^2}\left(\frac{\sqrt{3}a^2}{8}\right) \\
&= -\pi/3.
\end{aligned}$$

We have shown a linear vector potential (symmetric/centered about the y-axis) can host MZMs on a minimal Kitaev triangle's base corners. In general, this should be true for any odd function used

Triangle Length and Vector Potential Strength

For a staggered vector potential like the Heaviside or even a Tanh function we do not need to adjust the vector potential strength relative to its size. When considering larger Kitaev triangles we need to adjust the vector potential strength for linear and higher order vector potentials. Start with the botton left corner point, x_j, and look at its nearest neighbor along $\theta = \pi/3$, we denote this point with position x_l. If we look back at the path integral of a linear function we have the general form of

$$\begin{aligned}\phi_{jl} &= A\int_{x_j}^{x_l}\frac{dy}{dx}xdx \\ &= \frac{\sqrt{3}A}{2}(x_l^2 - x_j^2) = \pi/3.\end{aligned}$$

We can rearrange to get

$$A = \frac{2\pi}{3\sqrt{3}}\frac{1}{x_l^2 - x_j^2}. \tag{2.14}$$

A more simplified solution follows. For the outer length of a triangle we use `nr` to denote the number of rows the triangle has, it is one of the first few defined variables in a given script. The positions x_j and x_l have simple linear relations in regards to `nr`. Due to the equilateral nature of our triangle and centering about the y-axis

$$x_l = \frac{-a}{2}(\texttt{nr} - 1). \tag{2.15}$$

It's easy to see that $x_l = x_j + a/2$ which gives

$$x_l = \frac{-a}{2}(\mathtt{nr} - 2). \tag{2.16}$$

Now, the difference of the squares is

$$x_l^2 - x_j^2 = \frac{-a^2}{4}(2\mathtt{nr} - 3). \tag{2.17}$$

Plugging back into our expression we find

$$-\frac{8\pi}{3\sqrt{3}a^2(2\mathtt{nr} - 3)}. \tag{2.18}$$

This is expression is easy to implement in code.

2.3 Full Kitaev Triangle

A quick note on why we use hollow triangular islands. With the above gauge potentials present upon an equilateral triangle of arbitary length MZMs host at two of the corners and there live many edge states with in the band gap. This energy spectra can be seen in Fig. 2.1, there appear to be many edge states near the zero-energy states. We would like to use hollow triangular islands instead for two reasons: (1) $W \ll L$ is required for bulk-edge correspondence based on 1D topology to hold; (2) A finite W is needed to gap out the chiral edge states of a 2D spinless *p*-wave superconductor, i.e. opens a clean gap for the MZMs to host and braid in.

2.4 Minimal Kitaev Triangle

We next show that the minimal Kitaev triangle suffices to demonstrate braiding of MZM. To this end we consider a closed path linearly interpolating between the following sets of values of

Figure 2.1: Full trianglular island with length $L = 25$ with a staggered vector potential described by Eq. 2.11

ϕ_{jl}:

$$
\begin{aligned}
(\phi_{12}, \phi_{23}, \phi_{31}) = \left(0, -\frac{\pi}{3}, -\frac{\pi}{3}\right) &\equiv \boldsymbol{\phi}_1 \\
\rightarrow \left(-\frac{\pi}{3}, -\frac{\pi}{3}, 0\right) &\equiv \boldsymbol{\phi}_2 \\
\rightarrow \left(-\frac{\pi}{3}, 0, -\frac{\pi}{3}\right) &\equiv \boldsymbol{\phi}_3 \\
\rightarrow \boldsymbol{\phi}_1 &
\end{aligned}
\tag{2.19}
$$

It is straightforward to show that at $\boldsymbol{\phi}_2$ and $\boldsymbol{\phi}_3$ there are MZM located at sites $3, 1$ and $2, 3$, respectively. Therefore the two original MZM at sites $1, 2$ should switch their positions at the end of the adiabatic evolution.

Indeed, Fig. 2.2 shows that the MZM stays at zero energy throughout the parameter path that interchanges their positions. To show that such an operation indeed realizes braiding, we explicitly calculated the many-body Berry phase of the evolution and found the two degenerate many-body ground states acquire a $\frac{\pi}{2}$ difference in their Berry phases as expected. Compared to the minimum T-junction model with four sites, our Kitaev triangle model only requires three sites to achieve braiding between two MZM, and is potentially also easier to engineer experimentally. In the next section we will show that a more mesoscopic hollow-triangle structure can achieve similar results and may be preferred in other materials platforms.

2.5 Hollow Kitaev Triangles

For systems with less fine-tuned Hamiltonians than the minimal model in the previous section, it is more instructive to search for MZM based on topological arguments. In this section we show that MZM generally appear at the corners of a hollow triangle, which can be approximated by joining three finite-width chains or ribbons whose bulk topology is individually tuned by the same uniform vector potential.

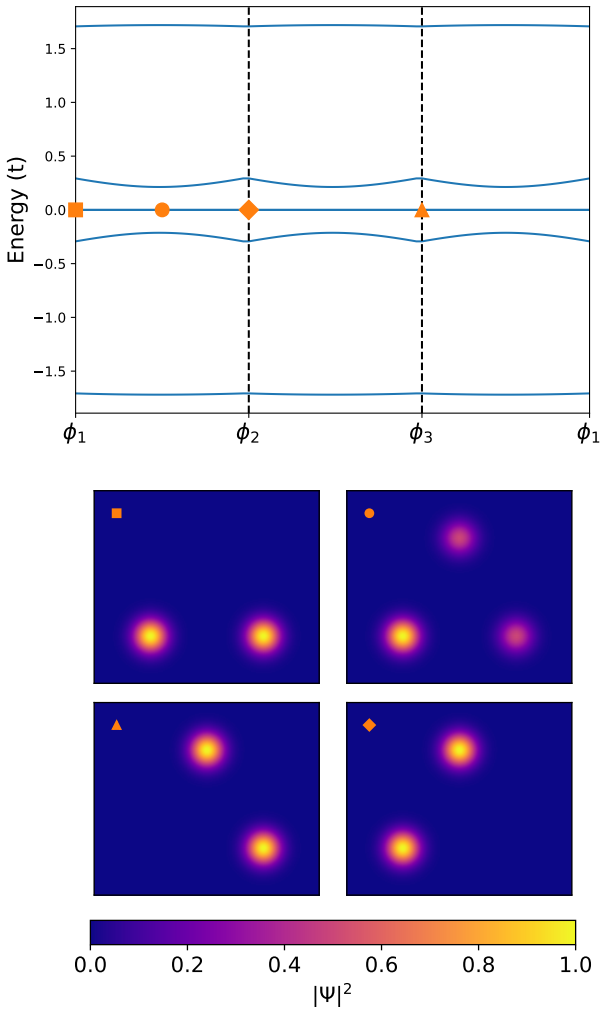

Figure 2.2: (a) Evolution of the eigenvalues of the 3-site Kitaev triangle along the closed parameter path for ϕ on the three edges. (b) MZM wavefunctions at different points of the parameter path. Clockwise from the upper left panel: $\boldsymbol{\phi}_1 \to \frac{1}{2}(\boldsymbol{\phi}_1 + \boldsymbol{\phi}_2) \to \boldsymbol{\phi}_2 \to \boldsymbol{\phi}_3$.

To this end, we first show that topological phase transitions can be induced by a vector potential in a spinless p-wave superconductor ribbon. In comparison with similar previous proposals that mostly focused on vector potentials or supercurrents flowing along the chain

Consider Eq. (2.2) on a triangular lattice defined by unit-length lattice vectors $(\mathbf{a}_1, \mathbf{a}_2) = (\hat{\mathbf{x}}, \frac{1}{2}\hat{\mathbf{x}} + \frac{\sqrt{3}}{2}\hat{\mathbf{y}})$ with W unit cells along $\mathbf{a}_2$ but infinite unit cells along $\mathbf{a}_1$, and assume the Peierls phases are due to a uniform vector potential $\mathbf{A}$ so that $\phi_{jl} = \mathbf{A} \cdot \mathbf{r}_{jl}$. We also introduce $\mathbf{a}_3 \equiv -\mathbf{a}_1 + \mathbf{a}_2$ for later convenience. The Hamiltonian is periodic along x and can be Fourier transformed through $c^\dagger_{m,n} = \dfrac{1}{\sqrt{N}} \sum_k c^\dagger_{k,n} e^{-ikm}$, where m, n label the lattice sites as $\mathbf{r}_{m,n} = m\mathbf{a}_1 + n\mathbf{a}_2$.

The resulting momentum space Hamiltonian can be written as the following block form up to a constant

$$\begin{aligned} \mathcal{H} &= \frac{1}{2}\sum_k \Psi_k^\dagger \begin{pmatrix} h_t(k) & h_\Delta(k) \\ h_\Delta^\dagger(k) & -h_t^*(-k) \end{pmatrix} \Psi_k \\ &\equiv \frac{1}{2}\sum_k \Psi_k^\dagger H(k) \Psi_k \end{aligned} \tag{2.20}$$

where $\Psi_k \equiv (c_{k,1}, \ldots, c_{k,W}, c_{-k,1}^\dagger, \ldots c_{-k,W}^\dagger)^T$. $h_t(k)$ is a $W \times W$ Hermitian tridiagonal matrix with $(h_t)_{n,n} = -2t\cos(k + \mathbf{A}\cdot\mathbf{a}_1) - \mu$ and $(h_t)_{n,n+1} = -t\left(e^{i(-k+\mathbf{A}\cdot\mathbf{a}_3)} + e^{i\mathbf{A}\cdot\mathbf{a}_2}\right)$. $h_\Delta(k)$ is a $W \times W$ tridiagonal matrix with $(h_\Delta)_{n,n} = -2i\Delta\sin k$ and $(h_\Delta)_{n,n\pm1} = \mp\Delta\left[e^{-i(\pm k + \frac{2\pi}{3})} + e^{-i\frac{\pi}{3}}\right]$.

By transforming Eq. (2.20) to the Majorana basis using the unitary transformation:

$$U \equiv \frac{1}{\sqrt{2}} \begin{pmatrix} 1 & 1 \\ -i & i \end{pmatrix} \otimes I \tag{2.21}$$

where I is a $W \times W$ identity matrix, and defining $A_k \equiv -iUH(k)U^\dagger$, not to be confused with the vector potential, one can calculate the Majorana number

In Fig. 2.3 (a) we show the topological phase diagrams for a 1D ribbon with width $W = 1$, $\mathbf{A} = A\hat{\mathbf{y}}$ and $\mathbf{A} = A(\frac{\sqrt{3}}{2}\hat{\mathbf{x}} + \frac{1}{2}\hat{\mathbf{y}})$ superimposed (see below). We found that the vector potential component normal to the ribbon length direction has no effect on the Majorana number, nor does the sign of its component along the ribbon length direction. However, topological phase transitions can be induced by varying the size of the vector potential component along the ribbon, consistent with previous results

To show that corner MZM indeed appear when the conditions given by the phase diagram Fig. 2.3 (a) are met, we directly diagonalize the BdG Hamiltonian of a finite hollow triangle with edge length $L = 50$ and width $W = 1$. Fig. 2.3 (b) shows the spectral flow (BdG eigen-energies evolving with increasing vector potential A) close to zero energy at chemical potential $\mu = 1.6$.

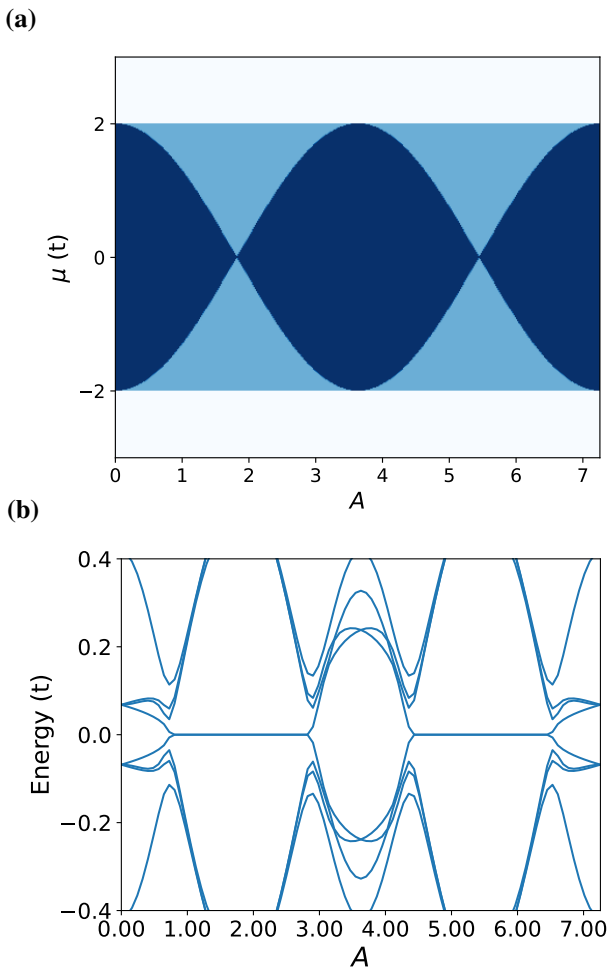

Figure 2.3: (a) Topological phase diagram for a $W = 1$ triangular chain with the Hamiltonian Eq. (2.20) obtained by superimposing the $\mathcal{M}(A, \mu)$ plots of 1D chains with $\mathbf{A} = A\hat{\mathbf{y}}$ and $\mathbf{A} = A(\frac{\sqrt{3}}{2}\hat{\mathbf{x}} + \frac{1}{2}\hat{\mathbf{y}})$. Color scheme: white—$\mathcal{M} = 1$, dark blue—$\mathcal{M} = -1$, light blue—$\mathcal{M} = 0$ (b) Near-gap BdG eigen-energies vs A for a finite triangle with edge length $L = 50$, $W = 1$, and $\mu = 1.6$.

Indeed, zero-energy modes appear in the regions of μ and A consistent with the phase diagram (except when the bulk band gap is too small; see

We finally show that rotating the uniform vector potential in-plane can manipulate the positions of the MZM without hybridizing them with bulk states for certain ranges of μ and A. Fig. 2.4 (a) plots the spectral flow versus the in-plane azimuthal angle of $\mathbf{A}$, which clearly shows that the zero-energy modes persist throughout the rotation and the bulk gap never closes. Figs. 2.4 (b-d) plot the BdG wavefunctions of the MZM at special values of φ. One can see that the two MZM appear to cycle through the three vertices by following the rotation of $\mathbf{A}$. The robustness of the

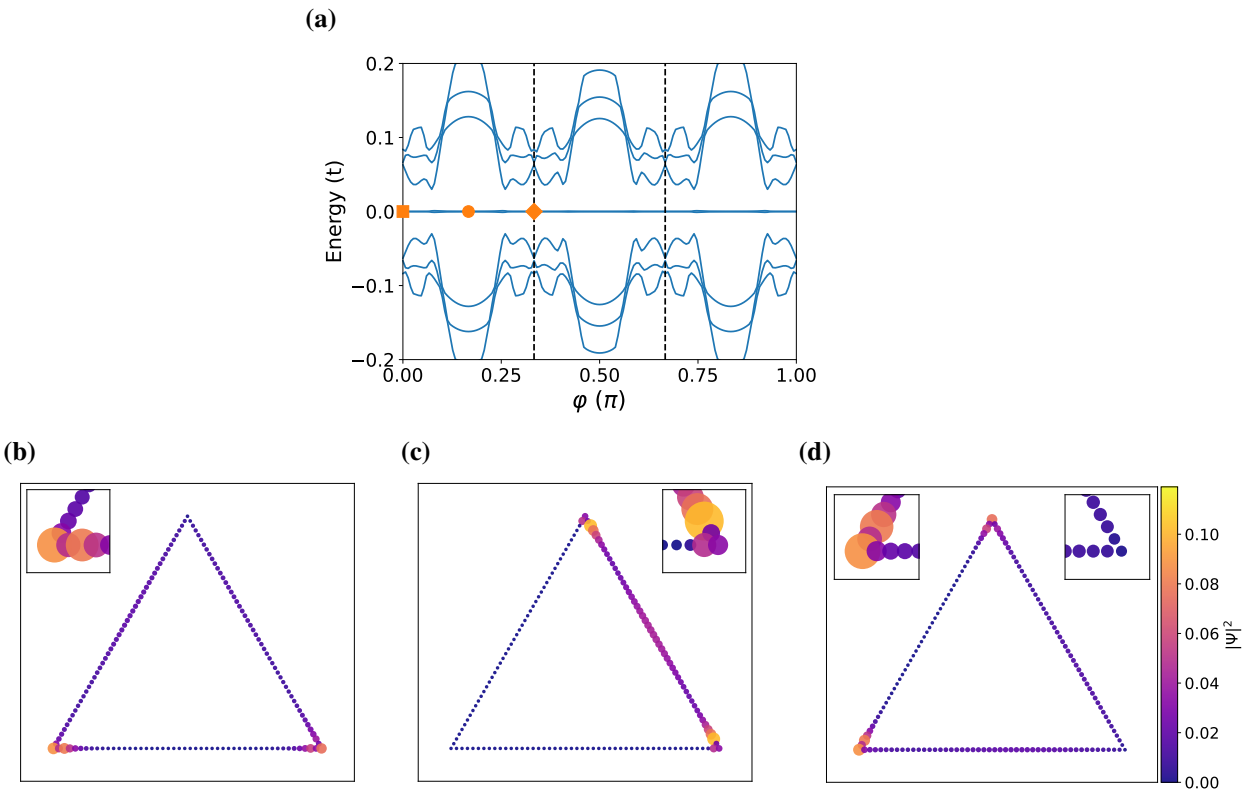

Figure 2.4: (a) Spectral flow of a hollow triangle with $W = 1$, $L = 50$, $\mu = 1.6$, and $A = 2.75$ with increasing rotation angle φ, defined through $\mathbf{A} = A(-\sin\varphi\hat{\mathbf{x}} + \cos\varphi\hat{\mathbf{y}})$. (b-d) BdG eigenfunction $|\Psi|^2$ summed over the two zero modes at $\varphi = 0$, $\frac{\pi}{6}$, and $\frac{\pi}{3}$, respectively.

MZM therefore requires the condition of two edges being in a different topological phase from the third one to be satisfied throughout the rotation. Such a criterion combined with the individual phase diagrams of the edges can help isolate the desired parameter regions of μ and A. We also note that the positions of the MZM do not interchange after φ increases from 0 to π, different from the situation of the minimal Kitaev triangle in Fig. 2.2. The reason is that the MZM in the latter case are not due to bulk-boundary correspondence [the values of $A = \frac{2\pi}{3\sqrt{3}}$ and $\mu = 0$ are a critical point in the phase diagram Fig. 2.3 (a)]. While the positions of the MZM at special points along the parameter path in the hollow triangle case have to be additionally constrained by the bulk topological phases of the three edges, that for the Kitaev triangle have more flexibility and are also protected by the finite size of the system.

./ch-02/chapter-02-cite

Chapter 3

Floquet Landau Levels

1. Introduction (Tahir's intro is fine, maybe in my own words, Floquet engineering)
    i Time dependent, motivation—QAHE gap but not QHE gap
    ii Floquet Theorem— quasi-energy spectrum
2. Results
    i square + A(t) (Tahir's perturbative calc)
    ii honeycomb + A(t) (Tahir's perturbative calc)
3. Discussion and future

Chapter 4

Conclusion and Discussion

What makes gauge potential unique in creating/tuning/manipulating new topoglical systems

Applications

Appendix A

Suitable Name

1. Majorana Number derivation

2. Other derivations not included in introduction

./ch-02/chapter-02-cite